Dynamical small-scale magnetic islands as a source of local acceleration of particles in the solar wind

Olga V. Khabarova[1], Gary P. Zank[2,3], Gang Li[2], Jakobus A. le Roux[2,3], Gary M. Webb[2], Olga E. Malandraki[4], Valentina V. Zharkova[5]

1. Heliophysical Laboratory, Pushkov Institute of Terrestrial Magnetism, Ionosphere and Radiowave Propagation RAS (IZMIRAN), Troitsk, Moscow 142190, Russia
2. Center for Space Plasma and Aeronomic Research (CSPAR), University of Alabama in Huntsville, Huntsville, AL 35805, USA
3. Department of Space Science, University of Alabama in Huntsville, Huntsville, AL 35899, USA
4. IAASARS, National Observatory of Athens, GR-15236 Penteli, Greece
5. Department of Mathematics and Information Sciences, Northumbria University, Newcastle upon Tyne, NE2 1XE, UK

E-mail: habarova@izmiran.ru

Abstract. We present observations of energetic particle flux increases up to 1 MeV at 1 AU, which cannot be associated with ordinary mechanisms of particle acceleration, such as acceleration at shocks or at the Sun. Such unusual energetic particle events very likely have a local origin. Multi-spacecraft observations show that numerous cases of energetic particle flux enhancements and spikes correspond to passages of spacecraft through areas filled with magnetic islands with a typical width ~0.01–0.001AU that experience dynamical merging or/and contraction. The presence of magnetic islands inside magnetically confined cavities in the solar wind may lead to local particle energization, especially in the case when the particles have already been pre-accelerated to keV energies, for example, at shocks or due to magnetic reconnection at the heliospheric current sheet. We consider different magnetic configurations that provide favourable conditions for both the appearance of small-scale magnetic islands and their confinement.

1. Introduction

Small-scale magnetic islands with a typical size of l ~0.01 AU or less are commonly observed in the solar wind plasma at 1 AU. The crossing of a certain magnetic island lasts from minutes to hours, but, in contrast to large-scale magnetic islands (or magnetic clouds), small-scale magnetic islands exhibit some grouping. Areas filled with small-scale magnetic islands, sometimes called flux ropes, can be observed for days [1]. The interplanetary magnetic field (IMF) strength increases and the plasma density decreases inside magnetic islands. The main features of these structures are a rotating magnetic field and the presence of small-scale current sheets at their borders.

Magnetic islands are often related to magnetic reconnection. The probability of their observation increases as the heliospheric current sheet (HCS) is approached [1], which is not surprising. Indeed, there are some signatures of magnetic reconnection that re-currently occur in many places on the HCS and determine specific properties of the plasma and magnetic field in the vicinity of the HCS [2].

Recently, we showed that magnetic islands near the HCS can experience merging and contraction [3], which may serve as a source of particle acceleration (as discussed in theoretical studies [4, 5, 6]). Magnetic island merging dominates near the HCS if it is undisturbed by high-speed flows or corotating interaction regions (CIRs). A specific rippled profile of the HCS confines magnetic islands and forms a tokamak-like structure that provides the possibility of additional energization of pre-accelerated particles [3]. Such an approach solves the problem of hypothetical low effectiveness of particle acceleration directly at 1 AU. Particle acceleration by magnetic island dynamics seems to play a significant role, because some crossings of the HCS are associated with energetic particle flux enhancements up to 1 MeV, which can be observed for many hours around the sector boundary crossing. We supposed that the energy gained by particles depends both on the reconnection rate and the local profile of the HCS. The reconnection rate increase, which produces more magnetic islands, may occur due to the impact of interplanetary coronal mass ejections (ICMEs) or corotating interaction regions (CIRs). The small-scale wavy, rippled and distorted HCS confines magnetic islands and accelerate particles more effectively than the plain or large scale wavy-shaped HCS. The combination of these features can produce strong particle acceleration.

Contraction of magnetic islands can take place everywhere, because the solar wind is a dynamic medium, but this process is most effective during HCS-ICME interactions. In this case there is (i) strong compression: (ii) plasma confinement between the ICME front and the HCS, and (iii) intensification of magnetic reconnection at the HCS due to its interaction with the ICME. As a result, one can observe strong energetic particle flux enhancements, sometimes comparable with energies typical for strong solar energetic particle SEP events [3].

The way to identify small-scale magnetic islands was shown in [1, 7]. The Grad-Shafranov reconstruction of flux ropes can help with understanding the local structure of magnetic fields (see ftp://ftp.iwf.oeaw.ac.at/pub/moestl/publicgscode/GS_handbook_june_2014.pdf and [8]), but it has some limitations, is not easy to perform, and sometimes is not exact. At the same time, a hodogram method [3] can help by providing a quick visual inspection of the analyzed events, simply using regression plots to reveal the IMF rotation inside magnetic islands. This supposes that if the rotation is obvious, one can see a half-circle in one of the planes B_r-B_t, B_t-B_n or B_r-B_n during the crossing of one island. Here and below, indices r, t and n correspond to radial, tangential and normal directions in the RTN coordinate system. At 1 AU, $r = -x$ in the GSE system, which is related to the ecliptic plane. The crossing of two islands or a chain of islands usually gives a full circle or many circles. The anti-correlation of a pair of the IMF components in combination with changing correlation between the density and the IMF during several hours may indicate a passage through the chain of magnetic islands as well.

We provide here support for theory and simulations [4, 5, 6], showing signatures of particle energization related to the occurrence of magnetic islands inside specifically confined regions of expanding solar wind. An explanation of observed time-intensity profiles of energetic particle fluxes through particle energization in merging/contracting magnetic islands for the case of the HCS-ICME interaction as well as for the crossing of the isolated HCS can be found in the recent publication [3]. In this work we will show cases of HCS-CIR and unusual HCS-ICME interactions. The shock fronts of CIRs which have fully developed beyond ~ 2 AU have been typically considered as the main source of energetic particle enhancements observed at 1 AU, with the particles, associated with the Reverse CIR shock beyond the spacecraft to be streaming towards the Sun [9, 10].

Magnetic islands are often observed in the turbulent area behind interplanetary shocks, which may represent a source of additional acceleration of particles in this area. Theoretical aspects of this phenomenon are considered in [4, 6]. Observations show that interplanetary shocks are usually accompanied by current sheets, and the shock itself always coincides with a sharp change in the IMF clock (azimuthal) angle. We will discuss a case when an interplanetary shock was observed close to the HCS and smaller current sheets.

As a whole, the work is aimed at showing the importance of taking into account the local structure of the IMF and the presence of dynamical small-scale magnetic islands, which are poorly-investigated natural accelerators of particles at the Earth's orbit.

2. Observations of energetic particle flux enhancements associated with the occurrence of small-scale magnetic islands

In our previous study [3] we showed that energetic particle flux increases are observed simultaneously with the occurrence of magnetic islands near the HCS. Here we will extend our multi-spacecraft study to cases when magnetic islands occur in between magnetic walls (represented by current sheets) and plasma boundaries (CIRs, ICMEs, shocks).

The local configuration of the IMF at 1 AU determines acceleration processes to a higher degree than is usually expected [3]. Therefore, it is important to analyse the whole picture of the ICME (or CIR) interaction with the HCS. The SMEI (Solar Mass Ejection Imager) can provide us with the necessary nearly whole sky data for the period from 2003 to 2011. A detailed description of the restored velocity/IMF plots obtained from STELab interplanetary scintillation data as well as the solar wind density plots from SMEI will be given below. The role of current sheets in the confinement of magnetic islands and the impact of high density (or the total pressure) on observed time-intensity profiles of energetic particle fluxes will be discussed as well.

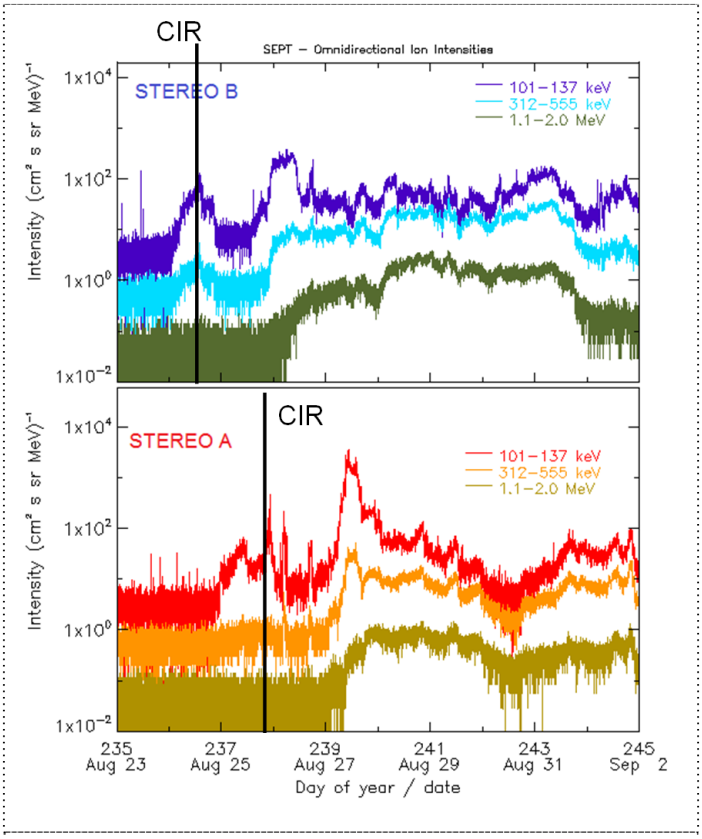

Figure 1. An increase in ion flux with energies up to 500 keV before the CIR as measured by STEREO A and STEREO B.

2.1. The HCS – CIR interaction

Let us explore the role of local CIR-associated particle acceleration on the formation of time-intensity profiles of suprathermal particle fluxes. We investigate whether the bounding of HCS- associated

magnetic islands by the HCS from one side and the CIR front from the other (which also contains local current sheets) may produce significant particle acceleration.

The energetic particle flux increases in August 2007 observed by the STEREO pair separated by 27 degrees (figure 1) were analyzed in [11]. These were not classical SEP events due to flares or acceleration at the ICME-related shock, but flux enhancements related to CIRs. The interesting point is that energetic particle flux enhancements were observed both before the first CIR's approach and between the two CIRs. The CIRs originated from (1) a long-lived low-latitude coronal hole, and (2) weak CMEs that did not hit the Earth directly (details can be seen in **1.avi** and **2.avi**). A classic explanation of the event, at which particles are supposed to be accelerated at reverse/forward shocks behind the Earth, was given in [11].

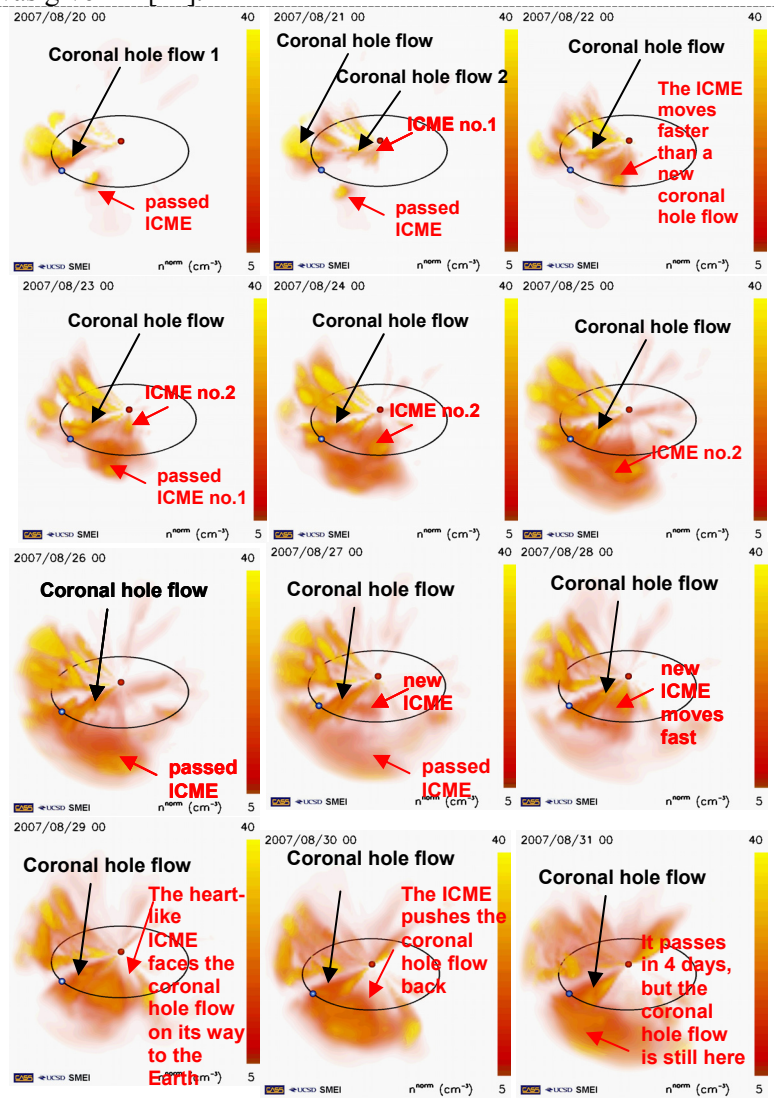

Figure 2. Daily snapshots of the solar wind density from the Sun to the Earth as observed by SMEI for the time period corresponding to Figure 1. The energetic particle flux profiles shown in Figure 1 are determined by interaction of the coronal hole flow and ICMEs that produce CIRs detected by the STEREO pair. The Earth's orbit is shown with the black ellipse, the Earth is the blue dot, and the Sun is the red thick dot in the centre. See 2.avi movie.

We are mainly interested here in the nature of the ion flux enhancements that occurred before the first CIR, which was not examined in [11]. The leading edge of the CIR, indicated by vertical lines in Figure 1, was observed in sequence by STEREO B and STEREO A. The separation angle between the STEREO pair was not very large, but, in contrast to typical SEP events, CIR-related energetic particle increases were detected by STEREO B and STEREO A with a time delay of many hours that corresponded to the rotation of the structure from the first spacecraft to the second one. Therefore, the observed changes in time-intensity energetic particle flux profiles were apparently determined by local configurations of the IMF.

A spatial distribution of the IMF from the Sun to the Earth's orbit may be reconstructed for the investigated period from the analysis of ground-based interplanetary scintillation data from the Solar Terrestrial Environment Laboratory (STEL), because the velocity profile approximately corresponds to the picture of the IMF spatial variations (see **1.avi**). One can find the corresponding 3D tomographic reconstructions performed with a 102-minute cadence and resolutions of 0.05 AU in height and 1^{o}x1^{o} in latitude and longitude on the page of The Solar Mass Ejection Imager (SMEI): http://smei.ucsd.edu/new_smei/data&images/data&images.html. SMEI itself viewed nearly the whole sky in visible light and provided the solar wind density profiles (for example, see **2.avi**). Generally, the solar wind density and velocity/IMF plots show different patterns: the plasma flows nearly radially outward from the Sun (**2.avi**), and the velocity/IMF pictures exhibit both rotation and expansion (**1.avi**).

During the period shown in figure 1, long-lived low latitude coronal holes were found side by side with active regions that produced weak coronal mass ejections (see the corresponding images at http://spaceweather.com/ and CME movies at http://sidc.oma.be/cactus/catalog.php). As a result, the flows interfaced in the solar wind and formed a sequence of CIRs and confined regions having delta (or nabla) shapes.

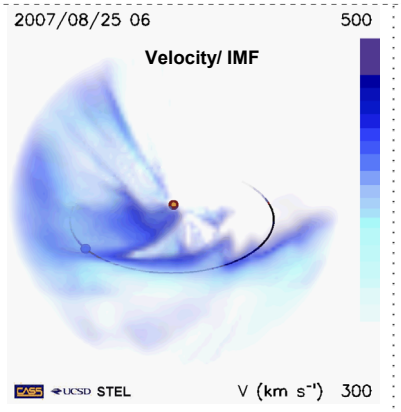

Figure 3. STEL measurements of the solar wind speed. ∇-shape cavities in the solar wind. See the 1.avi movie.

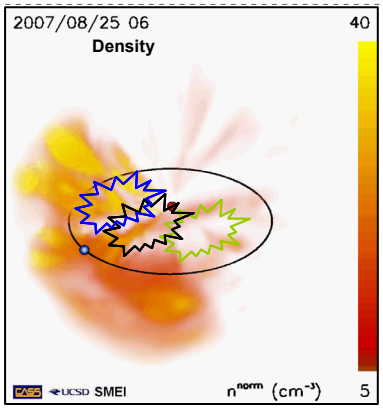

Figure 4. SMEI measurements of the solar wind density profiles that correspond to the speed/IMF cavities in figure 3. See the 2.avi movie.

The ∇-shape IMF cavities can be seen in the **1.avi** movie. Most streams are flowing from low-latitude coronal holes and sometimes face weak ICMEs. The streams of both kinds have different shapes, different speeds and different ways of propagation from the Sun to 1 AU. ICMEs propagate nearly radially and look like expanding balls (see figure 2), and streams from coronal holes resemble expanding tubes. As a result, at least three unusual ∇-shape IMF structures can be seen between the Sun and the 1 AU sphere at the same time (figure 3). Note that the upper side of ∇ is closer to the Sun than the narrow part, in contrast with a common view of the flows as V-shape structures that expand from the Sun [11].

The borders of each cavity shown in figure 3 are formed by the HCS and current sheets that belong to two different CIRs - passed and arriving ones (see the **1.avi** movie and figure 2). As we show below, such a magnetic cavity can confine dynamically changing magnetic islands, which results in local particle acceleration.

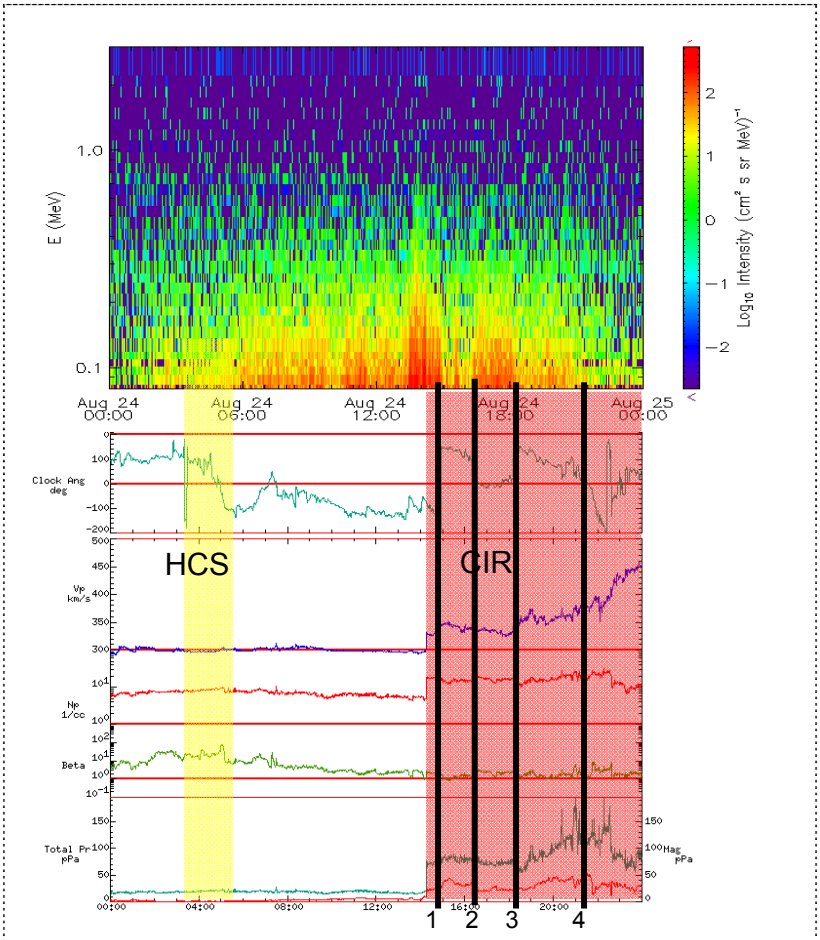

Figure 5. STEREO B observations showing the HCS crossing before the CIR. From top to bottom: energetic ion flux spectrogram, the IMF clock (azimuth) angle, the solar wind speed, the density, the plasma beta, the total (green) and magnetic (red) pressure. Energetic particle flux enhancements are seen in between the HCS (yellow stripe) and the CIR (pink stripe) as well as between current sheets inside the CIR (vertical lines).

Figure 2 shows SMEI measurements of the solar wind density in the visible light. SMEI was designed to observe ICMEs. It can show dense borders of ICMEs or flows from coronal holes (which are stream interaction regions – SIRs or CIRs). It cannot look inside ICMEs until they crossed the Earth orbit. CIRs from coronal holes are stable and conic-like, but ICMEs (even from weak CMEs), move faster, and produce ball-like "CIR-shells". Sometimes an ICME can move slower than plasma inside a coronal hole flow, but since the latter has a permanent source at the Sun, the entire picture looks like the ICME moves against the background of a stable slowly rotating stream. The changing density is partially responsible for what we see in blue velocity/IMF pictures (compare figure 3 and figure 4). On the other hand, velocity determines the IMF shape, so the whole picture of a particular event can be achieved by analysing both the combination of density and velocity plots.

Let us examine in detail the pre-CIR energetic flux enhancement shown in figure 1. Subsequent crossings of the HCS and the CIR are shown in figure 5. The IMF changed its direction approximately 10 hours before the CIR arrival (see the corresponding changes of the IMF clock (azimuth) angle). This was accompanied by a very high plasma beta and an increased plasma density in a background of low velocity. The yellow stripe shows the plasma sheet. The pink stripe indicates the CIR body. STEREO B detected a weak shock first, followed by significant density and velocity increases. The upper panel shows the energy of omni-directional ions (spectrogram).

Remarkably, the energetic ion flux enhancements occurred between the HCS and the CIR. Spikes in the spectrogram correspond to local magnetic islands. Even more remarkable is that the maximum increases in the flux are observed not exactly at the CIR-related shock, but in between local current sheets. Most strong current sheets inside the CIR are identified by numbers.

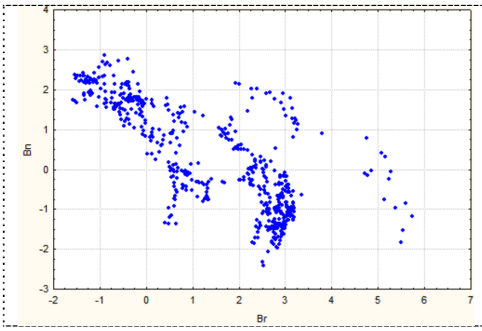

Figure 6. Hodogram of the IMF vector rotation in the B_n-B_r plane during the period of observations from the HCS crossing to the CIR crossing. 1-min STEREO-B IMF data, nT.

The rotation of the IMF vector inside magnetic islands located in the magnetic cavity between the HCS and the first strong CIR-related current sheet is shown in figure 6. In figure 5, one can see that the second prominent increase of the energetic ion flux occurs between the second and the third current sheet inside the CIR.

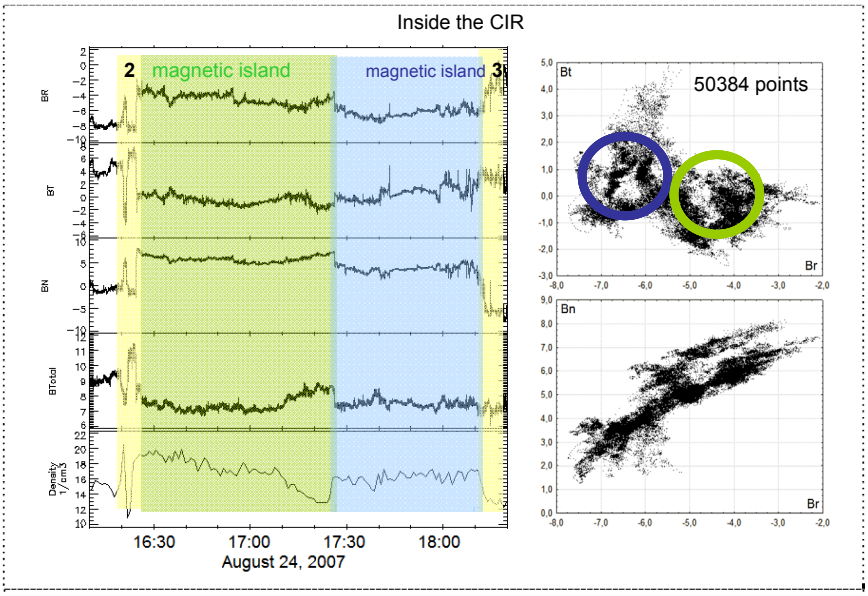

Figure 7. The IMF and density properties during the ion flux increase observed between current sheets 2 and 3 (see figure 5). Left figure, from top to bottom: three components of the IMF, the total *B* and the solar wind density. The right panel: similar to figure 6, but for R-T and R-N planes. High resolution data from STEREO B.

The behaviour of three IMF components, the total B and the solar wind density inside the magnetic islands as well as in the current sheets is shown in the left panel of figure 7. In the right panel of

Figure 7 we plot the hodogram of the IMF that shows the magnetic field vector rotation in two planes (B_r-B_t and B_n-B_r) inside two relatively large magnetic islands identified by the green and blue shading. The current sheets numbered 2 and 3 in figure 5 are shown in detail and marked with yellow stripes in figure 7. The magnetic islands are separated by a small-scale current sheet as well (the dark blue stripe).

The ACE spacecraft was located at the Lagrangian point in front of the Earth, and the separation angle with STEREO B was of 12°. ACE detected the passage of the whole structure several hours later. The HCS crossing, which is shown by the yellow stripe in figure 8, lasted longer in comparison with STEREO B, but the energetic ion flux behaviour was very similar. There was an area filled with magnetic islands in between the HCS and the first current sheet that belonged to CIR (line 1 in figure 8). An ion flux increase is observed in this area. Energetic ion fluxes measured by LEMS 120 on ACE show an increase many hours earlier than the CIR arrival at the Earth. The maximum is related rather to current sheet 1 than to the CIR shock.

STEREO A detected the CIR later than STEREO B, but the ion flux increase observed before the CIR leading front is even clearer and lasts longer (see figure 1). The bottom panel of figure 1 shows the omni-directional ion fluxes. However, if looked at more closely, the ion flux exhibits strong anisotropy. The upper panel of figure 9 shows fluxes of ions directed from the Sun. The bottom panel shows variations of the sunward ion flux. The HCS/plasma sheet crossing is indicated by the yellow stripe and the CIR shock is marked with the vertical line.

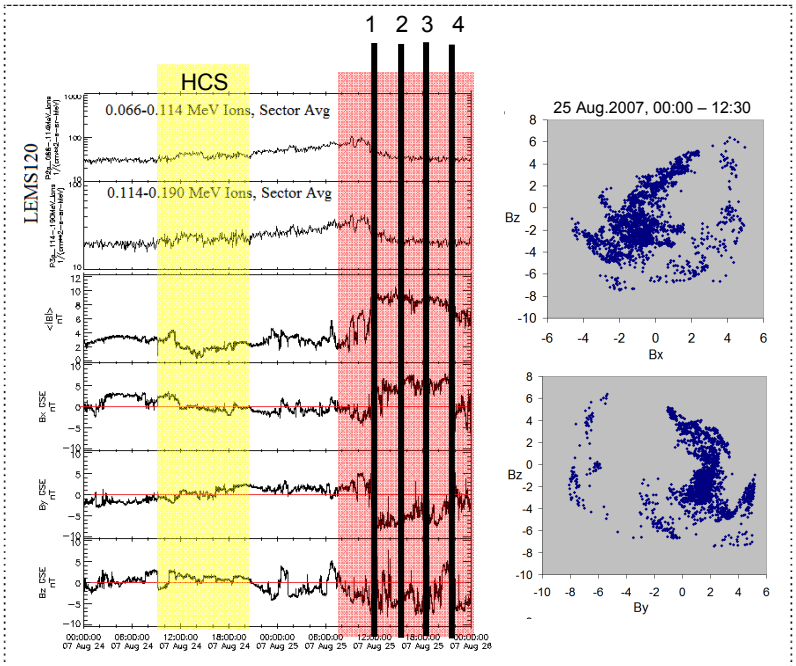

Figure 8. ACE observations during the event shown in figure 5. Left panel: energetic particle fluxes and the IMF components. Right panel: a hodogram of magnetic field rotation in the area between the HCS and the CIR (similar to figure 6 and figure 7, right panel).

The time-intensity ion flux profile is similar to that discussed above: an energetic ion flux increase is observed between the HCS and the leading edge of the CIR. It is clear that the first increase in energetic ion flux is due to 101-137 keV anti-sunward ions. This would not be possible if the particles originated from the CIR forward shock, as the dominant diffusive shock acceleration paradigm asserts, given that the shock is located at roughly 2-3 AU. Sunward accelerated ions, which could be from the forward shock, were detected many hours later. The interesting point is that the maximum sunward ion flux occurs after the shock crossing, which may be well related to results discussed in [6].

In summary, for the case that there are magnetic islands in the region in between the HCS and the CIR, the HCS-CIR interaction may produce energetic particle flux enhancements comparable with those observed during solar energetic particle (SEP) events. In the case discussed here, the magnetic islands were confined by the HCS and CIR-associated current sheets and compressed from at least one side by the approaching CIR.

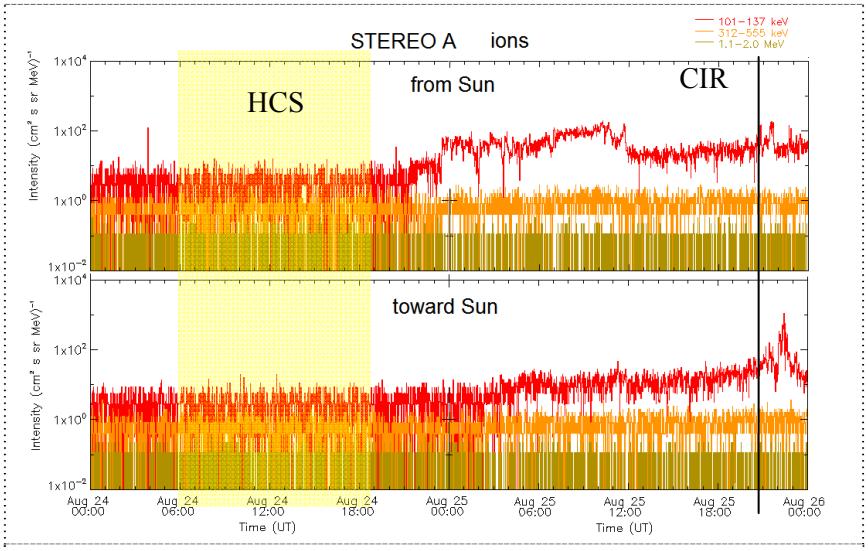

Figure 9. STEREO A observations of energetic particle flux enhancement before the CIR arrival. There was an approximately one day delay between the arrival of accelerated anti-sunward and sunward ions at the Earth.

2.2. The HCS-ICME interaction.

The HCS-CIR case examined above is rather similar to the HCS-ICME case discussed in [3]. The observational evidence points to the same underlying paradigm for particle acceleration that is favored because particles and magnetic islands are spatially confined by the HCS the approaching CIR or ICME. Two cases of the HCS-ICME interaction were considered in [3], terms of possible scenarios [12] of (i) the pre-existing HCS and (ii) the post-ICME crossing of the HCS, which was quickly restored after the passage of the ICME.

Sometimes we can observe at 1 AU very complicated cases with multiple CMEs that impact the HCS so strongly that it can no longer possesses a simple anymore, being rippled, and disrupted to a high degree or reconnected along the leading front of ICME. In STEL 3D velocity/IMF plots this appears as a temporary absence of the HCS in some places or the presence of multiple current sheets that resemble rose-leaves (see the **3.avi** movie). Let us consider cases when the HCS structure was very complicated due to a sequence of strong ICMEs that separated the HCS into many single current sheets.

The list of ICME events observed by STEREO A and B can be found at http://www-ssc.igpp.ucla.edu/forms/stereo/stereo_level_3.html . Event number 6 is an ICME detected by STEREO A on November 19, 2007. The magnetic obstacle (~ flux rope) starting time is indicated as 22:00 UT (the left vertical line in figure 10), and the end time is on November 21, 2007, 3:17 UT (the right line in figure 10). This period approximately corresponds to the growth and the main increase in the total pressure (figure 10, bottom panel).

The classification of the event as a clear ICME is arguable, because the velocity increase occurs after the “official” end of the magnetic cloud identified by Lan Jian, which is not typical for ICMEs,

though the IMF rotation in the magnetic cloud is very clear. However, one can see that neither the very high solar wind density nor the total pressure enhancement is associated with the energetic particle flux increase. On the contrary, two strong energetic ion flux enhancements are observed both before and after the passage of the large ICME-associated magnetic cloud characterised by the increased IMF strength and the solar wind density.

The first enhancement is most interesting, because there is absolutely nothing remarkable in the behaviour of parameters, which are usually considered to be responsible for particle acceleration: the solar wind speed decreases after the passage of the previous ICME, and there is no strong density increase during the energetic particle flux enhancements in different energy ranges as figure 10 shows. At the same time, the clock angle is changing frequently (the third panel from the top), which indicates the presence of multiple current sheets.

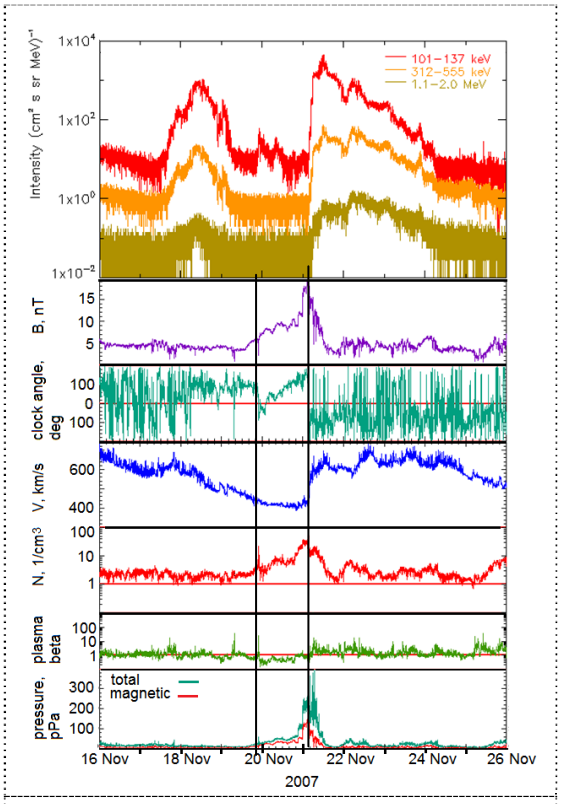

Figure 10. Case of a rippled HCS that surrounded an ICME. The energetic particle flux enhancements are observed not during the ICME, but in the areas filled with magnetic islands.

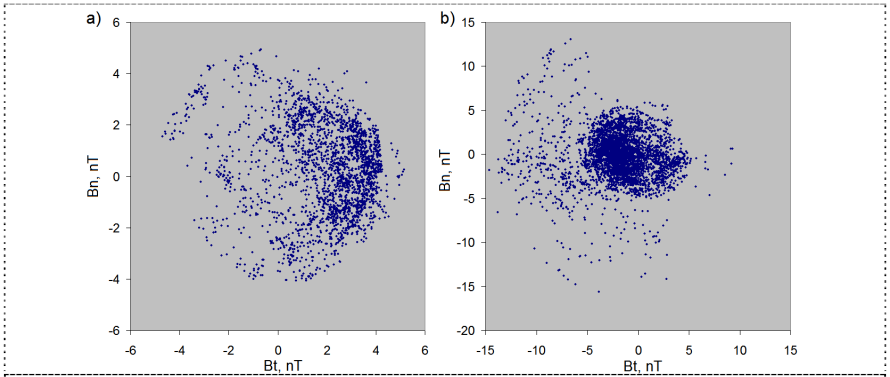

Figure 11. Rotation of the IMF that coincides with two strong energetic particle flux enhancements shown in figure 10 . STEREO A 1-min data.

We find that the observed frequent change of the IMF direction is due to the occurrence of multiple ripples on the HCS (see the **3.avi** movie). According to the 3.mpeg movie, the ICME was surrounded by the strongly disrupted and rippled HCS. The occurrence of small-scale magnetic islands inside the ripples is obvious from hodograms shown in figure 11.

Figure 11a corresponds to the first energetic ion flux increase seen in figure 10, and figure 11b shows the IMF vector rotation during the second energetic ion flux increase, which occurred after the passage of the ICME-related magnetic cloud. These enhancements were obviously local, because STEREO B detected them with some time shift, and the time-intensity profiles of the energetic ion fluxes were slightly different (not shown).

Do summarize, we emphasize again the importance of local IMF structure for confining and accelerating particles in the solar wind. In this case, particles accelerated at the ICME-related shock most likely could not propagate freely in the solar wind, being trapped by magnetic islands and confined by a very complicated HCS configuration. As a result, at 1 AU the picture became "inverted": areas where energetic ion flux enhancements are usually observed had no SEPs, but the surrounding HCS-related magnetic islands were full of accelerated particles.

2.3. The HCS-shock interaction

Interplanetary shocks (ISs) at 1 AU are usually associated with SIRs/CIRs or ICMEs, as seen from any shock list. An example can be found in paragraph 2.1. Thus ISs are followed by structures that may impact the HCS and change its configuration. This increases the reconnection rate at the HCS, produces more magnetic islands in some areas of the solar wind and, potentially, leads to local particle acceleration. The HCS is sensitive to the passage of an isolated interplanetary shock as well. Theoretically, the HCS is transparent for interplanetary shocks. At the same time, shocks may disrupt the HCS [13].

Observationally, it appears that the HCS tries to keep its form, but, being compressed by an interplanetary shock, it bends, moves forward and is then restored the shock passes. This process is clearly seen in STEL movies. If a spacecraft is close to the HCS, it detects the HCS crossing first, and then the IS crossing. The HCS restoration is seen as a second crossing of the HCS some time after the CS passage. This process has been poorly investigated observationally, although some simulations have been performed [13, 14]. Many questions regarding the state of the solar wind and energetic particles after IS passage throughout the HCS remain unanswered.

We know that ISs are followed by a turbulent wake that contains numerous magnetic islands [6, 14, 15]. If this is the case, the highly disturbed HCS may (i) retain the magnetic islands that are formed downstream of the IS, and (ii) produce more magnetic islands because of the increased reconnection rate. In any event, the traversal of the HCS by an IS may result in a prolonged highly turbulent state of the solar wind behind the shock (much more prolonged than in the case of an IS passage that does not interact with the HCS). An example of an IS interacting with the HCS is presented in figure 12.

STEREO A observed the crossing of an isolated interplanetary shock at 9:18 UT on May 19, 2008 (see the STEREO shock list at http://www-ssc.igpp.ucla.edu/forms/stereo/stereo_level_3.html). It is marked in figure 12 by the black vertical line. The solar wind density and speed indicate any presence of a structure that could contaminate the case significantly, except for the presence of the HCS. The main crossings of the HCS are indicated by the vertical red lines, and the areas of fluctuating IMF direction, which, similar to previous events, may be treated as the plasma sheet, are identified by yellow stripes.

The HCS crossing occurred several hours before the IS arrival at 1 AU. One can see the clock angle changes sharp and the plasma beta is very high (more than 100) during the HCS crossing. The IS pushed the HCS back and the spacecraft found itself again in the same sector as before the HCS crossing. The restoration of the HCS was detected several hours later.

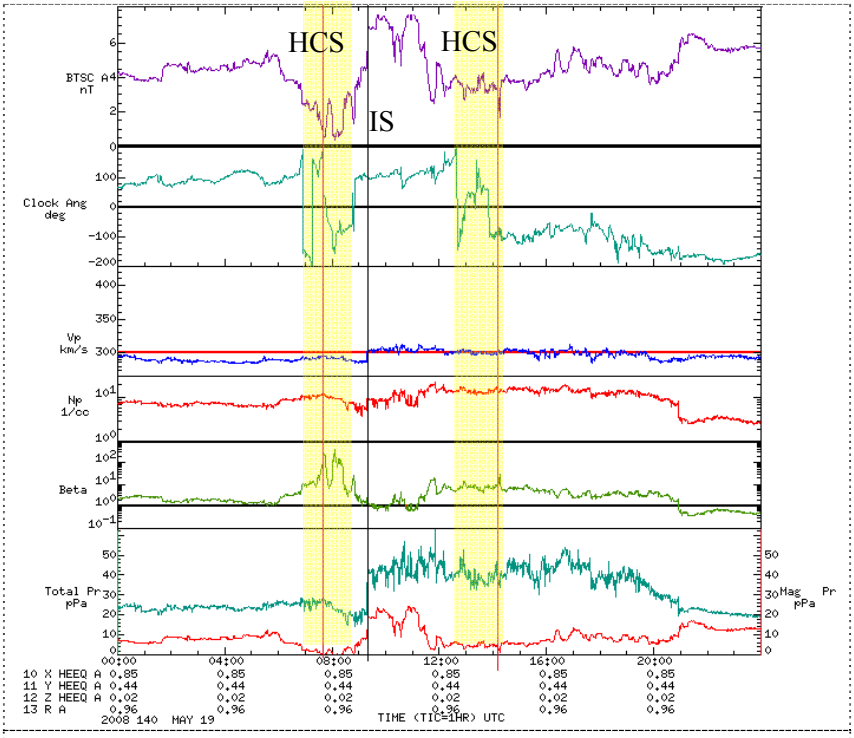

Figure 12. Plasma and magnetic field parameters for the case of the HCS-shock interaction (similar to figure 10). The shock is identified by the black line, and the main crossings of the HCS are indicated by red lines. STEREO A data.

The behaviour of suprathermal electrons (pitch angle distribution function PAD), the energetic ion dynamic spectrum, and the IMF component variations during the time period shown in figure 12 are illustrated in figure 13. The upper panel of figure 13 shows the running correlation coefficient between the tangential B_t and the vertical B_n components of the IMF (the time-window where the coefficient is calculated is 180 minutes, and the consequent shift is 1 minute).

The PAD function shows a wide area of fluctuations in the suprathermal electron propagation direction and a prolonged flux dropout that coincides with the HCS/plasma sheet crossing. It was discussed before [3] that such strong pitch angle scattering in the vicinity of the HCS is a signature of the occurrence of magnetic islands. The most prominent rotation of the IMF vector is observed in the T-N plane, and the negative correlation coefficient between B_t and B_n shows an approximate position of the islands along the time axis. It should be noted that periods of strong negative correlation coefficient coincide with the dropouts and periods of multidirectional propagation of suprathermal electrons.

Figure 13 clearly shows that the energetic ion fluxes increase most significantly behind the shock. Moreover, the maximum occurs exactly during the period of long-lasting electron flux dropout and pitch-angle direction isotropy observed after the second HCS crossing. This period is characterised by the presence of HCS-associated magnetic islands and rotating magnetic field as seen in figure 14.

This example shows that many unusual energetic particle events may be related to the interaction of the IS and the HCS due to the ability of the disrupted HCS to produce and confine magnetic islands in its vicinity. All the effects discussed in the theoretical models [4, 5, 6, 16] may be applied to this case, but the details of the HCS-shock interaction and peculiarities of particle acceleration that occur during this rather long process should be investigated further.

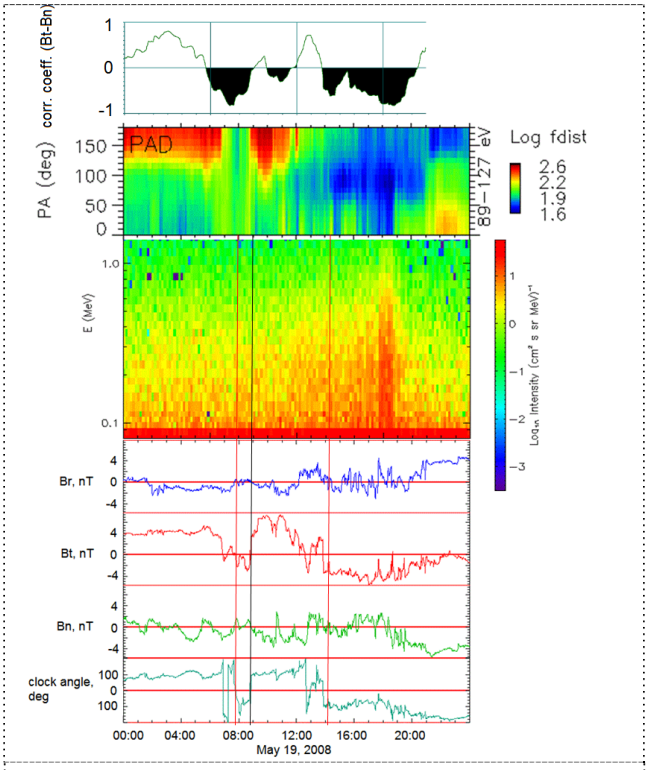

Figure 13. From top to bottom: The running correlation coefficient between B_t-B_n components, the suprathermal electron pitch-angle distribution function (spectrogram), the energy of ions (spectrogram). The main energetic ion flux enhancement occurs behind the shock (black line), which coincides with the electron heat flux dropout and corresponds to the largest magnetic island near the HCS. Measurements from STEREO A.

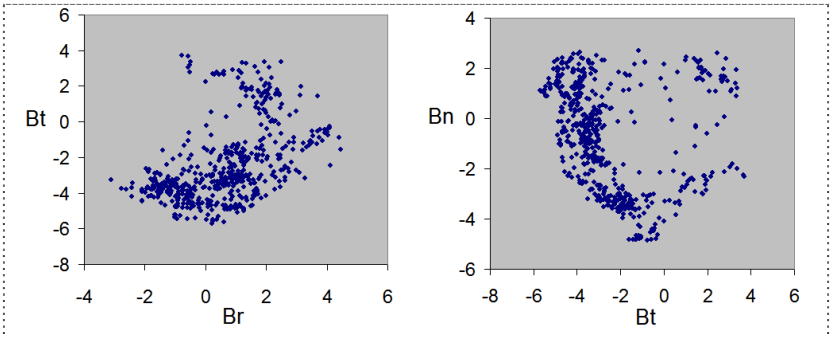

Figure 14. Hodogram of the magnetic field rotation behind the shock shown in figures 12 and 13.

3. Discussion and summary

In this case-study paper, we have shown examples of energetic particle enhancements observed near the Earth orbit that cannot be easily explained in terms of the dominant paradigm for the acceleration of particles to keV-MeV energies in the solar wind. The commonly accepted view for accelerating particles to these energies includes acceleration either at shocks or at the Sun. In both cases this occurs far from 1 AU, so an observer will see merely the result of various distant processes. However, numerous discrepancies between observations and the theoretical perspective stimulated us to seek other mechanisms that could explain energetic particle flux enhancements, as a result of local processes that occur directly at 1 AU and that can be traced by different spacecraft.

The application of a theory for particle energization by magnetic islands through their dynamical compression and merging [3, 4, 5, 6, 16] to observations introduces the possibility for solving many problems that traditionally arise in addressing the particle acceleration in the solar wind. Recently, we have shown that the heliospheric current sheet is a place near which magnetic islands permanently exist and evolve, experiencing both contraction and merging [3]. Both processes may occur simultaneously, but the dominant evolution depends on the local IMF configuration and such circumstances as approaching ICMEs, interplanetary shocks or CIRs. All shown examples of the HCS interaction with various structures suppose strong compression of magnetic islands either locked between two current sheets (the HCS and the strongest current sheet inside the ICME or the CIR) or produced by the IS impact.

In summary, the presence of the HCS near ICMEs, CIRs and ISs increases the probability of observing energetic particles accelerated up to 1 MeV.

(i) We have found evidence for significant particle energization in the ∇-shape magnetic cavity formed due to a stream interface. Single-point measurements show energetic ion flux enhancements that occur in an area filled with magnetic islands in between the HCS and the strongest current sheet inside the CIR.

(ii) Acceleration of particles to keV-MeV energies appears to occur inside CIRs as well if there are magnetic islands in between CIR-associated current sheets.

(iii) An increased solar wind density/total pressure is not a factor that determines strong particle acceleration (as seen from the HCS-ICME interaction case).

(iv) We confirmed that the occurrence of magnetic islands near the heliospheric current sheet results in electron pitch-angle scattering and prolonged heat flux dropouts.

(v) The most intensive energetic ion flux enhancements are observed not exactly at interplanetary shocks, but somewhere behind them. The maximum energetic ion flux increase is associated with current sheets surrounded by magnetic islands in the CIR case and with the post-shock restoration of the HCS and following magnetic islands in the case of an isolated shock.

(vi) The presence of the HCS makes the turbulent area behind the interplanetary shock wider because it keeps and additionally produces magnetic islands in its vicinity.

3.1. Acknowledgements

SMEI and STELab data were taken from the official website http://smei.ucsd.edu/new_smei/data&images/data&images.html. The corresponding movies (1.avi, 2.avi and 3.avi) can also be downloaded from http://files.olgakhabarova.webnode.com/200000049-c00d8c108d/1.avi, http://files.olgakhabarova.webnode.com/200000050-49c684ac0c/2.avi, http://files.olgakhabarova.webnode.com/200000051-3245f343a0/3.avi. The Solar Electron and Proton Telescope STEREO data were obtained from the http://www2.physik.uni-kiel.de/STEREO/index.php (University of Kiel, Germany), and other STEREO data were provided by the STEREO science center: http://stereo-ssc.nascom.nasa.gov/data.shtml. High-resolution ACE data were taken from the official Goddard Space Flight Center OMNIweb plus Web site: http://omniweb.gsfc.nasa.gov.

We acknowledge the partial support of NASA grants NNX08 AJ33G, Subaward 37102-2, NNX09AG70G, NNX09AG63G, NNX09AJ79G, NNG05EC85C, Subcontract A991132BT, NNX09AP74A, NNX10AE46G, NNX09AW45G, and NNX14 AF43G, and NSF grant ATM-0904007. O.V.K. was supported by RFBR grant 14-02-00769 and partially by RFBR grant 14-02-00308. JAlR acknowledges support from NASA grants NNX14AF43G and NNX15AI65G. O.E.M. received funding from the European Union's Horizon 2020 research and innovation program under grant agreement No 637324.

References

[1] Cartwright M L and Moldwin M B 2010 *J. Geophys. Res.* **115** A08102
[2] Zharkova V V and Khabarova O V 2012 *Astrophys. J.* **752** 35
[3] Khabarova O, Zank G P, Li G, le Roux J A, Webb G M, Dosch A, Zharkova V V and Malandraki O E 2015 *Astrophys. J.* in press
[4] Zank G P, le Roux J A, Webb G M, Dosch A, and Khabarova O 2014 *Astrophys. J.* **797** 28
[5] le Roux J A, Zank G P, Webb G M and Khabarova O 2015 *Astrophys. J.* **801** 112
[6] Zank G P, Hunana P, Mostafavi P, le Roux J A, Li G, Khabarova O, Cummings A, and Stone E *J. Phys.:* Conf Series this volume
[7] Moldwin M B, Ford S, Lepping R, Slavin J and Szabo A 2000 *Geophys. Res. Lett.* **27** 57
[8] Hu Q and Sonnerup B U Ö 2001 *Geophys. Res. Lett.* **28** 467
[9] Malandraki O E, Marsden R G, Tranquille C, Forsyth R J, Elliott H A, Lanzerotti L J, and Geranios A 2007 *J. Geophys. Res.* **112**, A06111
[10] Gómez-Herrero R, Malandraki O, Dresing N, Kilpua E, Heber B, Klassen A, Müller-Mellin R, and Wimmer-Schweingruber R F 2011 *JASTP* **73** 551
[11] Wu Z, Chen Y, Li G, , Zhao L L, Ebert R W, , Desai M I, Mason G M, Lavraud B, Zhao L, Y , Liu C-M, Guo F, Tang C L, Landi E and Sauvaud J **2014** *Astrophys. J.* **781** 17
[12] Manchester W B IV, van der Holst B and Lavraud B 2014, *Plasma Phys. Control. Fusion* **56** 064006
[13] Hu Y Q and Jia X Z *J.* 2001 *Geophys. Res.* **A12** 29299
[14] Odstrcil D, Dryer M and Smith Z 1996 *J. Geophys. Res.* **101** 19973
[15] Tessein J A, Matthaeus W H, Wan M, Osman K T, Ruffolo D and Giacalone J 2013 *Astrophys. J. Lett.* **776** L8
[16] le Roux J A , Webb G M, Gary P Zank and Khabarova O *J. Phys.*: Conf. Series this volume